Sixth International Symposium on Marine Propulsors
SMP'19, Rome, Italy, May 2019

A Lagrangian analysis of scale effects on sheet cavitation inception

Martijn van Rijsbergen[1], Simon Beelen[2]

[1]Maritime Research Institute Netherlands (MARIN), Wageningen, The Netherlands
[2]formerly of MARIN

ABSTRACT

Sheet cavitation on foils and propellers is often initiated by free-stream bubbles. Consequently, scale effects on cavitation inception occur due to differences in the bubble spectrum (size vs. concentration), propeller diameter and rotation rate. To better understand the sensitivities, a 2D Lagrangian tracking method is used to compute the trajectories and radial dynamics of free-stream bubbles that cause cavitation on a blade section. Systematic series of conditions are computed by varying the initial radius and the initial position of a bubble. It is shown that the range of initial bubble radii that can cause cavitation decreases from 0.03 to at least 600 μm for a full-scale propeller, to 5 – 160 μm for a small propeller model. If sufficient bubbles in this size range are present in a cavitation facility, this does not explain why sheet cavitation inception is often inhibited on model-scale propellers. However, the bubble dynamics computations did show significantly less bubble growth on the small propeller model.

Keywords

Sheet cavitation inception, bubble dynamics, scale effects.

1 INTRODUCTION

Sheet cavitation inception depends – next to a local pressure below the saturated vapour pressure – on the characteristics of the fluid, solid surface and flow. For example, a lack of nuclei, negligible surface roughness or a laminar boundary layer can inhibit cavitation inception, induce isolated spots of cavitation or travelling bubbles instead of a continuous sheet cavity. Because these inception effects seem to be more pronounced on model scale than on full scale, they are often designated as 'scale effects'.

Scale effects on cavitation inception have been studied for decades, mostly in an experimental way (Billet & Holl, 1981). A drawback in many experiments is the inability to vary a single parameter. For example, when changing the rotation rate of a propeller at a constant cavitation number, the boundary layer on the blade changes as well as the free-stream bubble spectrum. Consequently, viscous effects on cavitation inception will be mixed with water quality effects.

Alternatively, computations can be used to study specific scale effects, provided that the relevant physical mechanisms are adequately modelled. Johnson & Hsieh (1966) studied the effect of the velocity and the size of a two-dimensional half body on the size range of free-stream bubbles that could enable cavitation inception using a quasi-steady computational model. They introduced the screening effect as the mechanism that pushes large bubbles away from the stagnation point, thus preventing them from reaching the point of minimum pressure and cause cavitation inception.

Kuiper (1981) considered screening of free-stream nuclei as a possible explanation for the inhibition of sheet cavitation inception on a propeller model, but did not study it further. Van Rijsbergen & van Terwisga (2010) found a significant effect of free-stream nuclei on sheet cavitation inception on the same propeller model as used by Kuiper. Without seeding, the rotation rate had a strong effect on the amount of sheet cavitation. A conceptual model – including screening – related the decrease in rotation rate to a decrease in the background nuclei size range that could induce sheet cavitation inception. Both the input values as well as the model were considered to give trends and an order of magnitude only.

A more precise evaluation of the bubble screening effect was made by Beelen & van Rijsbergen (2018). An equation of motion of a bubble was coupled with a bubble dynamics equation and applied to 2D potential flows. The simulations showed that for a symmetric flow – like the half body studied by Johnson and Hsieh – screening occurred for large bubbles that were pushed over the low pressure region. For an asymmetric flow – as occurs over a section of a propeller blade – larger bubbles could still reach the low pressure region if they started at a particular location below the dividing streamline. The range of vertical positions where bubbles could start, however, decreased with increasing bubble size. Quasi-static limits were derived which matched the ranges of initial radii and positions of bubbles that reached their critical radius – as obtained by the dynamic simulations – very well. The explosive growth of a bubble beyond its critical radius is associated with vaporous cavitation (Brennen, 1995).

In the present paper, the Lagrangian tracking method of Beelen & van Rijsbergen (2018) is used to study scale effects on sheet cavitation inception for a 2D blade section of propeller 'S' (Kuiper, 1981). In particular the relation with the free-stream bubble size distribution and cavitation inception mechanisms is studied and discussed.

2 METHOD

The 2D Lagrangian trajectory method with bubble dynamics of Beelen & van Rijsbergen (2018) is used to compute cavitation inception events – induced by free-stream bubbles – on or near a 2D hydrofoil. The equation of motion includes the forces due to acceleration, Kelvin impulse, drag, pressure gradient and gravity. The history force which was originally included in the model, has not been taken into account here, since it is less relevant in this 2D application (Beelen and van Rijsbergen, 2018). The bubble dynamics is described by the Keller-Miksis equation and the potential flow field is derived from a Kármán-Trefftz transformation.

The impact model – which describes the behaviour of a bubble when it hits the surface of the cavitating object – has been updated to resemble experimental observations more closely (see e.g. Guennoun *et al.*, 2003). Instead of a bubble that remains spherical when in contact with the surface, in the visualization it gradually transforms into a hemisphere. In the bubble dynamics computations, however, we work with an equivalent spherical bubble (with the same volume) using the pressure at the centre of mass of the deformed bubble. Since the centre of mass of a hemispherical bubble is located at $3/8^{th}$ of its radius from the surface, a lower pressure is experienced. Furthermore, the new impact model uses a more stable and efficient solver for the bubble dynamics equation, which enables continuation of the computation during a bubble implosion and rebound.

3 SET-UP

The effect of free-stream nuclei on sheet cavitation inception has been studied experimentally on propeller S by (Kuiper, 1981), (Gindroz and Billet, 1998) and (van Rijsbergen and van Terwisga, 2010). A 2D blade section of propeller S at a relative radius r/R = 0.6 is taken here for the Lagrangian tracking computations. A simple method has been used to find a 2D equivalent flow condition of the 3D flow around the rotating propeller. A wetted-flow computation using PROCAL (a boundary element method developed at MARIN) was made of the propeller at advance coefficient, J = 0.4. The PROCAL pressure distribution at r/R = 0.6 was taken as a reference. Both the angle of attack and the camber of the 2D blade section were changed to fit the pressure distribution as well as possible, see Figure 1. Only the pressure distribution of the first percent of the chord, including the minimum value, could not be fitted. Due to the limited number of panels in the PROCAL computation and the limited possibilities of the Kármán-Trefftz method to change the leading edge geometry, it was decided to accept the obtained fit as a good representation of the 3D situation.

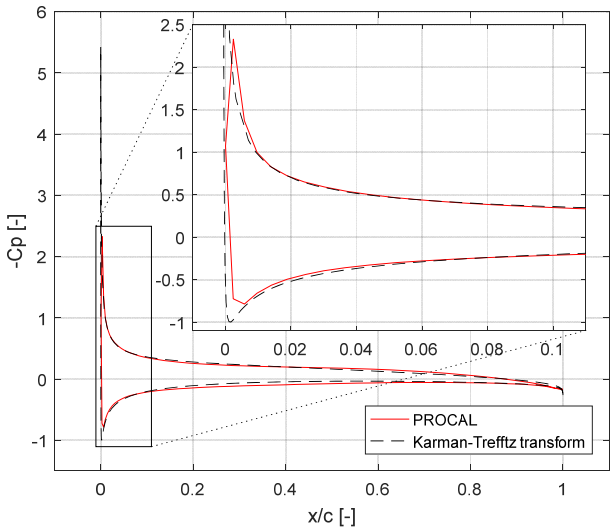

Figure 1: Fitted pressure coefficient using the equivalent blade section (using pressure coefficient Cp and horizontal position x, non-dimensionalized with chord length c).

The computations were performed in a standard 2D reference frame where the nose-tail line of the foil was held horizontally and the incoming flow has an upward inclination (i.e., a positive angle of attack), see Figure 2. Bubbles are – one by one – released from a vertical line located 0.77 c upstream of the leading edge, each at a different vertical position.

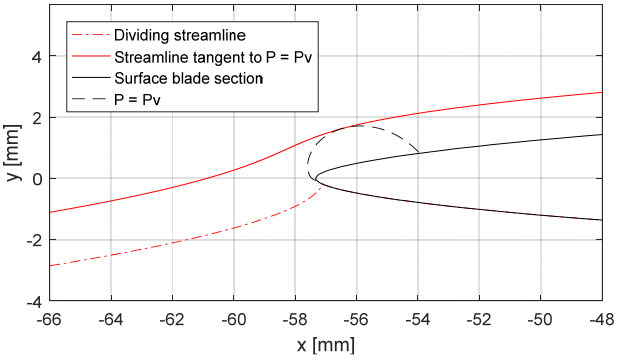

Figure 2: Blade section with P = P_V contour, dividing streamline and streamline tangent to the P = P_V contour (with pressure P and vapour pressure P_V).

4 RESULTS

Systematic variations of initial bubble radius and initial vertical position were made at two cavitation numbers for combinations of three propeller diameters at four rotation rates. The blade section (defined by r/R = 0.6) and angle of attack (defined by J = 0.4) are kept constant. The results are discussed in the sections below.

4.1 Initial bubble radius and position

Figure 3 shows a systematic variation of the bubble initial radius and vertical position relative to the blade section. It shows where a bubble of a certain size should start to induce sheet cavitation. The propeller diameter (D = 0.34 m) and its rotation rate (n = 10 Hz) are typical of model-scale tests and the chosen cavitation number (σ_n = 2.2) gives a limited form of sheet cavitation. Three regions can be distinguished. The diagonal (curved) band, running

from the top left corner, to the bottom right corner, contains conditions that lead to cavitation. The region above it contains conditions where the bubble arrives at or above the suction side of the blade section, but without causing cavitation. The region below the diagonal band contains all the initial conditions which result in a bubble ending up at the pressure side of the blade section, again without causing cavitation. Three cavitation categories are distinguished: a bubble reaches its critical radius (red asterisk); a bubble reaches its critical radius and hits the surface in the region where the pressure is below the vapour pressure (black square); or a bubble hits the surface in the region where the pressure is below the vapour pressure (green asterisk). The first category leads to bubble cavitation. Bubbles in the second and third category can induce sheet cavitation depending on the surface and boundary layer characteristics. The effect of distributed leading-edge roughness is taken into account by considering a distance to the blade section less than 50 µm as hitting the surface.

For illustration, the trajectories and radial dynamics of six microbubbles are shown as insets. Case 1 has an initial bubble radius of 19 µm, cases 2-4 have initial bubble radii of 50 µm and cases 5-7 have initial bubble radii of 160 µm. The bubble in case 1 starts just below the dividing streamline, but crosses it just upstream of the leading edge of the blade section and arrives at the suction side of the blade section close to the point of minimum pressure. Since it touches the surface and grows beyond its critical radius (0.54 µm), it is likely to cause sheet cavitation inception. Due to inertia effects, the maximum equivalent radius (1.33 mm) is reached at a position where the pressure is already far above the vapour pressure. This higher pressure causes the bubble to collapse fiercely, approximately 12 mm downstream.

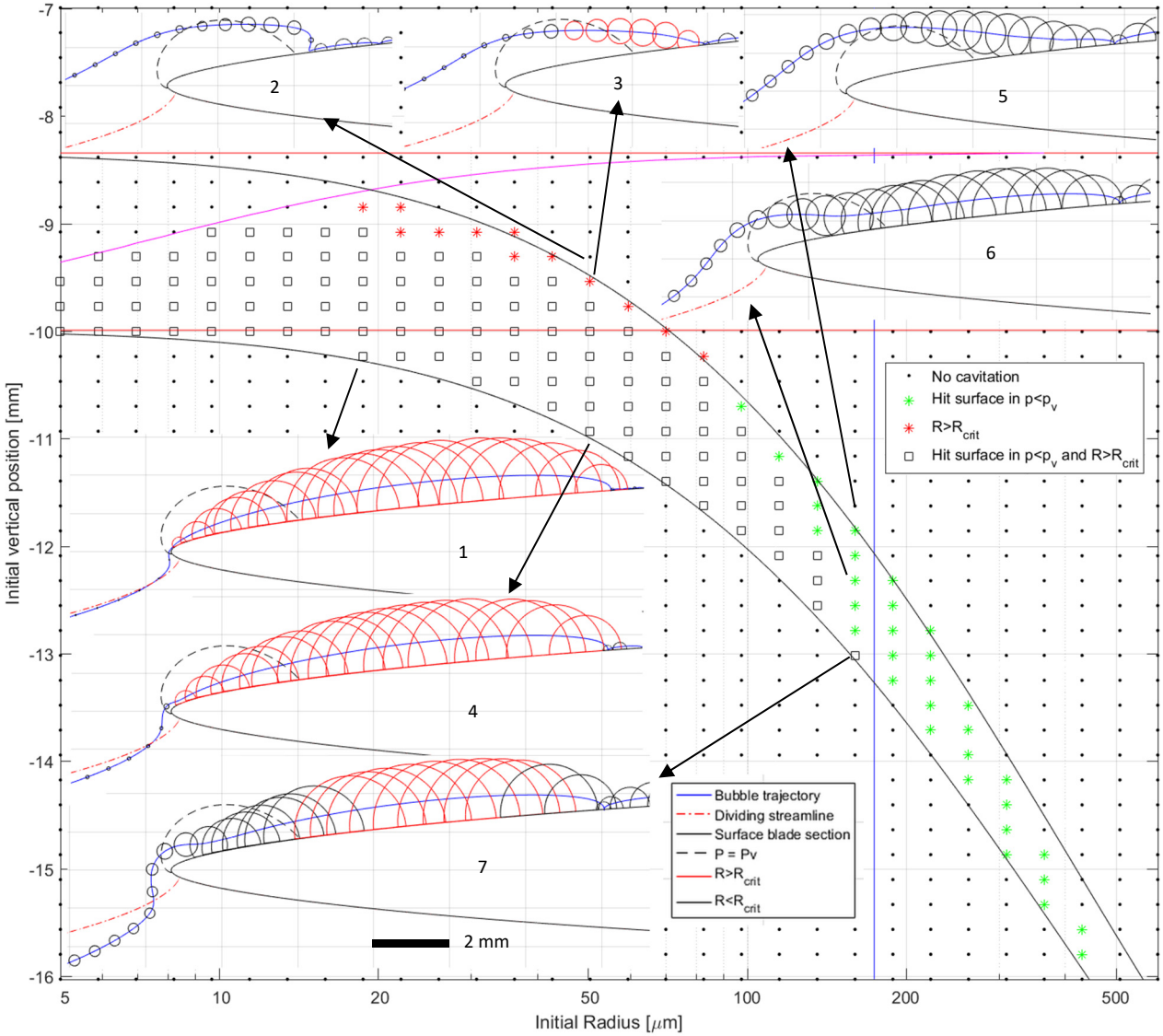

Figure 3: Overview of initial conditions of bubbles (initial radius, R_0 between 5 and 600 µm) that can cause cavitation inception on the r/R = 0.6 blade section of propeller S with D = 0.34 m and n = 10 Hz (Reynolds number Rn = $1.2 \cdot 10^6$) at σ_n = 2.2. The trajectories and radial dynamics of six microbubbles are shown as insets. The critical radius is denoted Rcrit.

Case 2 shows a bubble which just enters the region where the pressure is below the vapour pressure (indicated by the dotted black line). This causes the bubble to grow, but the local pressure does not decrease below the critical pressure of the bubble and therefore it does not reach its critical radius. When the bubble leaves the low pressure region, it starts to respond to the region's attractive force, implodes and is directed towards the surface. This movement is due to the Kelvin impulse (Blake, Leppinen and Wang, 2015). Conservation of the Kelvin impulse increases the magnitude of the relative velocity of the bubble when it collapses. Because the bubble is moving slower than the surrounding liquid in the direction of the surface, it retracts and accelerates towards the surface. After its rebound, the bubble is advected with the flow. The bubble in case 3 starts only 0.2 mm lower, but this causes the bubble to experience a pressure below its critical pressure long enough to let the bubble grow beyond its critical radius (indicated in red). The bubbles in cases 2 and 3 do touch the surface of the blade, but in a region where the pressure is above the vapour pressure. The bubble in case 4 starts just high enough to reach the suction side of the blade. It grows beyond its critical radius (0.21 mm) to a maximum equivalent radius of 1.31 mm and collapses at approximately the same position as the bubble in case 1. Case 5 shows a bubble that enters the region where the pressure is below the vapour pressure at roughly the same location as the bubble in case 2 – although it started at a lower initial position. Due to its larger added mass, it responds slower to the low pressure region. No sheet cavitation is induced because the bubble touches the blade in a region above the vapour pressure. The bubble in case 6 experiences a minimum pressure below its critical pressure, but because of its relatively large size it does not reach its critical radius. It does, however, touch the surface in the region where the pressure is below the vapour pressure. With sufficient surface roughness, a sheet cavity can then be generated (van Rijsbergen and van Terwisga, 2011). Case 7 shows a bubble which, like the bubbles in cases 1 and 4, barely reaches the suction side of the blade. But once it does, it starts to grow rapidly. Due to its larger initial radius, however, its critical radius is also larger (1.11 mm). This value is reached at a position further downstream. Despite of a much larger initial radius, approximately the same equivalent maximum radius (1.29 mm) and point of implosion as the bubbles in cases 1 and 4 is obtained. The approximately constant maximum bubble size – independent of its initial size – has also been found by Ceccio and Brennen (1991). Brennen (1995) explained that both the asymptotic growth rate and the available time for growth are mainly a function of the pressure and are relatively independent of the initial bubble radius.

Finally, Figure 3 contains some lines that indicate limits and regions. The two horizontal red lines indicate the vertical positions at which the two streamlines – shown in Figure 2 – cross the initial horizontal starting position of the bubbles. The top red line indicates the streamline which is tangent to the contour of the vapour pressure. The bottom red line indicates the dividing streamline. The vertical blue line and the curved purple line are quasi static limits, derived by Beelen and van Rijsbergen (2018) and based on the Blake threshold (Brennen, 1995). The blue line indicates the *maximum* initial radius of a bubble that can reach its critical radius on the blade section by quasi-steady growth. It is based on the assumption that the maximum (critical) radius of a spherical bubble is equal to the maximum height of the region where the pressure is below the vapour pressure. The curved purple line indicates the *minimum* initial radius of a bubble that can reach its critical radius on the blade section by quasi-steady growth. First, it is assumed that these bubbles are small and hence follow a streamline. Second, the bubble's critical pressure is assumed to be equal to the minimum pressure along streamlines between the two red streamlines shown in Figure 2. The curved black lines are based on a combination of the deviation of small and large bubbles from their initial streamlines. The deviation of small bubbles is dominated by drag and the deviation of large bubbles is controlled by the pressure gradient and their inertia, due to added mass. The lower black line indicates the lowest initial vertical position of bubbles that reach the suction side of the blade section. The upper black line indicates the highest initial vertical position of bubbles that can reach the region where the pressure is below the vapour pressure. It is based on the lower line and a vertical shift that decreases from the height of the region where the pressure is below the vapour pressure for small bubbles to zero for an infinite bubble radius (Beelen and van Rijsbergen, 2018).

4.2 Rotation rate

Figure 4 shows the initial conditions for cavitation inception – similar to Figure 3, for the same propeller diameter and cavitation number – but for a lower rotation rate (7 Hz).

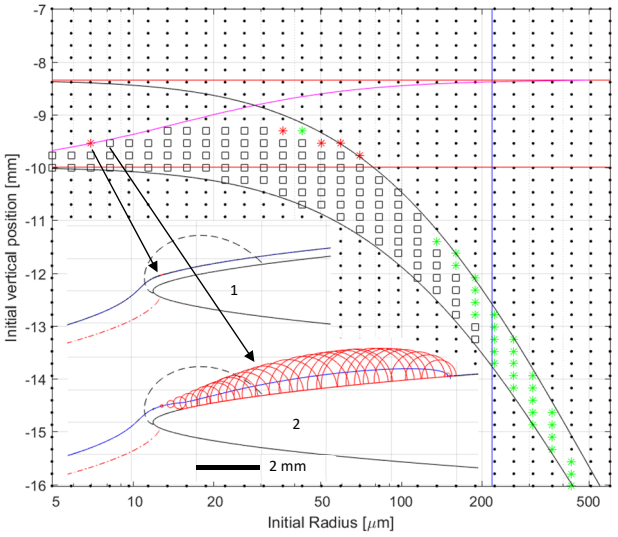

Figure 4: Initial conditions for cavitation inception, bubble trajectories and radial dynamics for σ_n = 2.2, D = 0.34 m and n = 7 Hz (Rn = $8.1 \cdot 10^5$). See Figure 3 for legends.

The dividing streamline stays at the same position since the angle of attack is the same. The $P = P_V$ contour as well as the streamline tangent to it, have the same location because the cavitation number is the same. The trajectories and radial dynamics of two bubbles with initial radii of 7 µm (case 1) and 8 µm (case 2) are shown in Figure 4. Both bubbles encounter approximately the same pressure history along their trajectory, which is below the critical pressures of the bubbles. The smallest bubble has, however, a lower critical pressure. Combined with the very short pressure peak this gives only sufficient time to grow just above its critical radius of 14 µm (see the small red part in the trajectory), before it collapses again. The largest bubble has a higher critical pressure, which gives it just enough time to grow significantly beyond its critical radius to a maximum equivalent radius of 0.88 mm. At this lower rotation rate, the ambient pressure is lower for the same cavitation number. Due to the lower local velocity, however, the net effect is a higher minimum pressure at the blade section, see Figure 5.

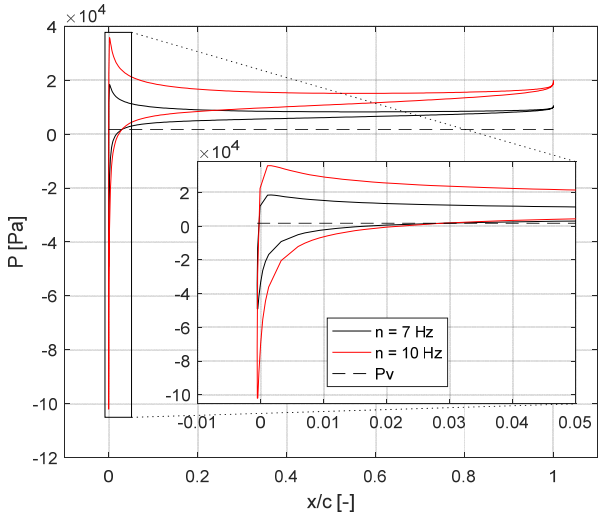

Figure 5: Pressure distribution at blade sections for n = 7 Hz and n = 10 Hz at the same cavitation number $\sigma_n = 2.2$.

Therefore, larger bubbles (with higher critical pressures) are needed which can grow beyond their critical radius. As a result, the magenta and blue lines shift to the right in Figure 4 (relative to Figure 3).

4.3 Bubble screening

Figure 6 shows a condition closer to inception ($\sigma_n = 4.0$) for the same propeller diameter and rotation rate as in Figure 4. A number of phenomena can be discerned. The dividing streamline stays at the same position, because the angle of attack has remained the same. The streamline tangent to the $P = P_V$ contour has moved downward due to a smaller region where the pressure is below the vapour pressure. As a result, the range of initial vertical positions where bubbles can start to generate cavitation inception has decreased relative to the condition in Figure 4.

The bubbles in cases 1 and 2 have initial radii of respectively 10 and 31 µm. These bubbles show approximately the largest expansions in this condition because they hit the surface of the suction side close to the leading edge. Both reach a maximum equivalent radius of approximately 0.4 mm and a distance between start of their growth and collapse of approximately 3 mm. If the contours of these bubble sequences would represent streaks of sheet cavitation, they would be just visible in a cavitation experiment. The bubble in case 3 has an initial radius of 160 µm. It is pushed around the leading edge, but it just touches the blade surface in the region where the pressure is below the vapour pressure. Therefore, it could induce sheet cavitation. This is the only vertical position from which a bubble of this size can start to generate sheet cavitation with a vertical grid spacing of 232 µm. Additional computations show that with steps of 11 µm, a range of 148 µm is found from where 160 µm bubbles can start to generate a sheet cavity. The bubbles in cases 4 and 5 have an initial radius of 189 µm. Their vertical initial positions are only 11 µm apart. Neither of these bubbles generate sheet cavitation inception, so the chance that bubbles with initial radii equal to or larger than 189 µm generate sheet cavitation inception is practically zero. This effect – which limits the maximum initial bubble size for sheet cavitation inception – is called screening (Johnson and Hsieh, 1966).

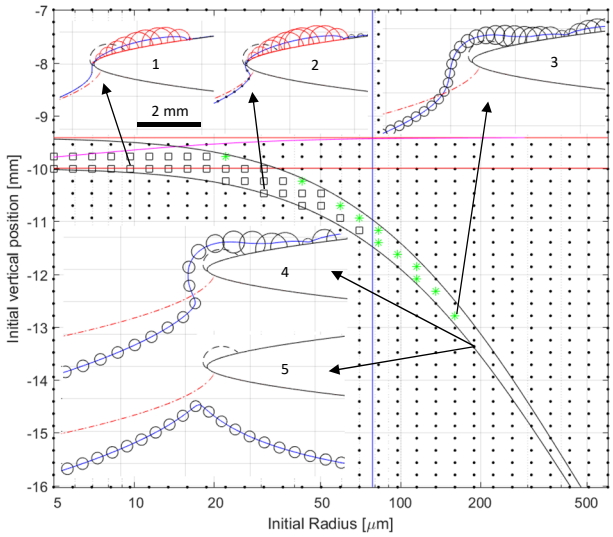

Figure 6: Initial conditions for cavitation inception, bubble trajectories and radial dynamics for $\sigma_n = 4.0$, D = 0.34 m and n = 7 Hz ($Rn = 8.1 \cdot 10^5$). See Figure 3 for legends.

4.4 Small model-scale propeller diameter

Figure 7 shows the initial conditions for cavitation inception for the same rotation rate and cavitation number as in Figure 6, but for a factor of two smaller propeller diameter (0.17 m). The initial vertical positions of the dividing streamline, the $P = P_V$ contour, and the streamline tangent to it also scale with a factor of two. Although the relative grid density has stayed the same, the number of initial conditions that lead to a bubble that surpasses its critical radius has decreased significantly relative to the larger propeller diameter. The shift to the right of the magenta line – indicating the minimum initial bubble radius that can reach its critical radius – corresponds well with this. Contrary to the computations for D = 0.34 m, the

blue line at R_0 = 69 μm - indicating the maximum initial bubble radius that reaches its critical radius according to a quasi-steady approach - does not correspond well with the value found from the simulations (36 μm). The series of bubbles starting 0.1 mm above the dividing streamline – indicated by a horizontal row of green asterisks – do not hit the blade section itself but touch the virtual roughness elements at the leading edge.

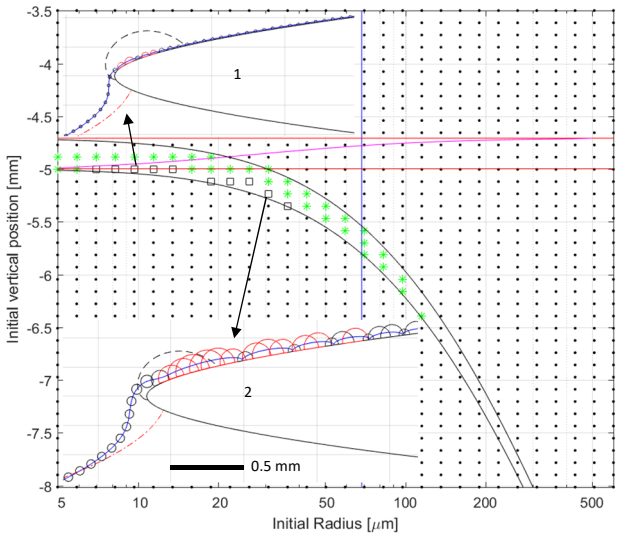

Figure 7: Initial conditions for cavitation inception, bubble trajectories and radial dynamics for σ_n = 4.0, D = 0.17 m and n = 7 Hz (Rn = $2.0 \cdot 10^5$). See Figure 3 for legends.

The bubble in case 1 with an initial radius of 10 μm experiences a minimum pressure below its critical pressure, but the pressure peak is not so low and long as for the propeller with D = 0.34 m, see Figure 8.

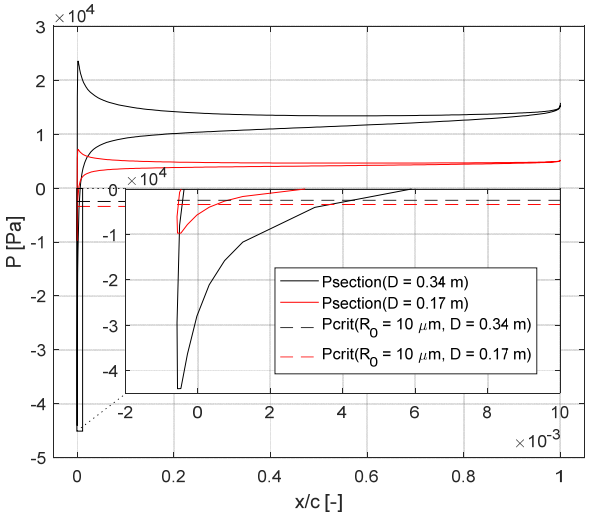

Figure 8: Pressure distribution at blade sections for D = 0.34 m and D = 0.17 m at the same cavitation number σ_n = 4.

Therefore, the bubble grows just beyond its critical radius (18 μm) to a maximum equivalent radius of 27 μm and collapses again. In an experiment with normal observation equipment, such a bubble will not be visible. A similar story holds for the bubble in case 2. Because of a slightly higher critical pressure, the bubble has some more time to grow, but still its maximum equivalent radius is 99 μm, which is much smaller than for the propeller with D = 0.34 m. Due to relative small growth ratio, the first implosion is not so fierce and the bubble keeps on rebounding while travelling approximately 5 mm before it attains its steady initial value again. The minimum initial bubble radius for which screening occurs (R_S) is 136 μm.

4.5 Full-scale propeller diameter

Figure 9 shows the initial conditions for cavitation inception for a typical full-scale propeller diameter and corresponding rotation rate at the same cavitation number as in Figure 7. The initial vertical positions of the dividing streamline, the P = P_V contour, and the streamline tangent to it, scale with the diameter ratio. Both the range of (scaled) initial vertical positions and the range of initial radii of bubbles that grow beyond their critical radius is larger than for the model-scale propellers. Furthermore, no screening occurs up to the maximum initial bubble radius of 600 μm. The magenta line has shifted to the left and out of view because the minimum pressure on the blade section is so low that even bubbles smaller than 0.1 μm start to cavitate. The insets show the trajectories of bubbles with initial radii of 10, 31 and 600 μm. The distance between the start of their growth and collapse is approximately 50 mm, which corresponds with the scaled-up lengths found on the large propeller model.

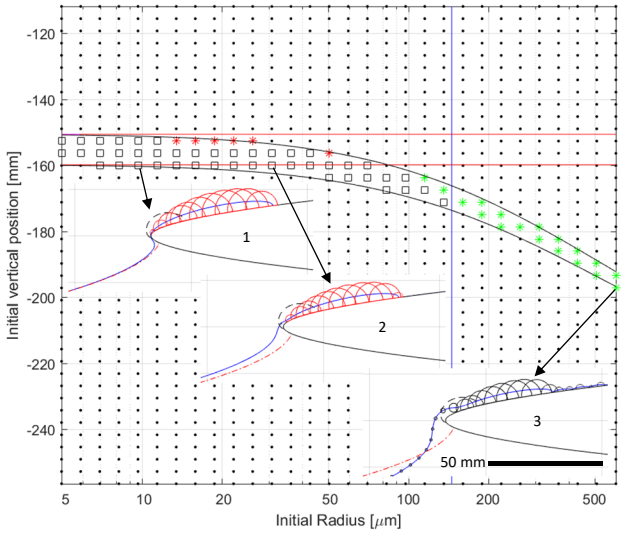

Figure 9: Initial conditions for cavitation inception, bubble trajectories and radial dynamics for σ_n = 4.0, D = 5.44 m and n = 3 Hz (Rn = $8.9 \cdot 10^7$). See Figure 3 for legends.

4.6 Bubble size spectra for sheet cavitation inception

Additional simulations were made for the model-scale propellers at n = 30 Hz and the initial bubble radii at which screening starts were determined. These are shown in Figure 10, together with the other minimum and maximum initial bubble radii that can induce sheet cavitation inception on a propeller blade section. The blue and green lines with asterisks are based on the initial bubble radii for which screening was found using the Lagrangian tracking computations for 7 and 30 Hz, respectively. The smallest initial bubble radius for which screening was found (98 μm) corresponds to a propeller diameter of 0.17 m at a

rotation rate of 30 Hz. No screening was found within the chosen size range at full scale. Therefore, a marker with an upward-pointing arrow is placed at initial radius, R_0 = 600 µm. A horizontal dashed black line with open squares indicates that in all Lagrangian tracking computations, the same minimum initial radius for sheet cavitation inception was found (5 µm and equal to the minimum value of the range studied). The magenta line indicates the quasi-steady limit, based on the Blake threshold and the minimum pressure coefficient of the blade section for a range of propeller diameters at a rotation rate of 7 Hz. The magenta open circle indicates the same limiting value for the full-scale propeller.

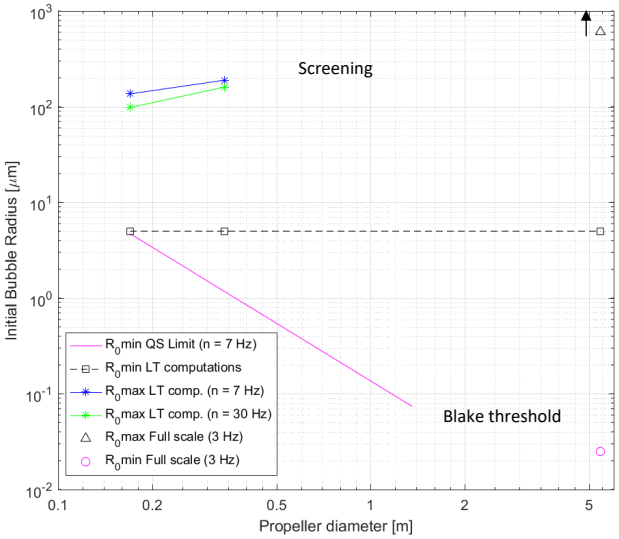

Figure 10: Limits of free-stream nuclei radii that can cause sheet cavitation inception for a range of propeller diameters at σ_n = 4.0. QS: Quasi-Steady LT: Lagrangian Tracking.

The horizontal dashed black line crosses the magenta line at D = 0.17 m and R_0 = 5 µm. This can also be seen in Figure 7. The Blake threshold has shown to be a reliable indicator for the minimum initial bubble radius for cavitation inception. So together with the radii at which screening was found, the range of free-stream nuclei that can induce sheet cavitation can be determined from Figure 10. On a full-scale propeller, bubbles with radii between 0.03 and at least 600 µm can induce sheet cavitation inception. This decreases on a model-scale propeller with D = 0.34 m to a range between 1 and approximately 200 µm. Finally, on a propeller model with D = 0.17 m, only bubble radii between 5 and 160 µm can cause sheet cavitation inception.

5 DISCUSSION

5.1 Limiting and indicating lines

The results of the quasi-steady model, indicating the minimum initial bubble radius that can reach its critical radius, (magenta line in Figure 3) agrees very well with the dynamic simulations in various conditions. Because the simulations take more time for smaller bubbles, this limit may be used in future sensitivity studies.

The quasi-steady model that indicates the maximum initial bubble radius that can reach its critical radius (blue line in Figure 3) is based on a spherical bubble. Still, it works quite well with the new impact model. This indicates that the attained bubble sizes strongly correlate with the dimensions (not necessarily only the height) of the region where the pressure is below the vapour pressure (Brennen, 1995). The only exception found is the smallest propeller diameter at the lowest rotation rate. Here, the quasi-steady assumption does not hold anymore, because the bubbles have insufficient time to grow (see Section 5.3).

The curved black lines represent the contours of the initial conditions that lead to sheet cavitation inception quite well from the smallest model scale to full scale. The lower black line still holds at the minimum initial bubble radius for which screening is found in the simulations (R_S). For bubbles slightly smaller than R_S, however, the upper black line starts to overestimate the initial vertical position of bubbles that can still reach the region where the pressure is below the vapour pressure, see Figures 3, 4, 6 and 7.

5.2 Bubble screening

Beelen and van Rijsbergen (2018) noted that for larger bubbles in a symmetrical flow (e.g. over a half body), the range of initial vertical positions – from which bubbles could start and reach the region where the pressure is below the vapour pressure – gradually decreases to zero with increasing bubble radius. For an asymmetrical flow (e.g. over a foil at an angle of attack), it was found that larger bubbles can still reach the region where the pressure is below the vapour pressure if they start at a particular location below the dividing streamline. It was assumed that the range of vertical positions where bubbles could start – to generate sheet cavitation – slowly decreased to zero for an infinite bubble radius. Implicitly, this would mean that for bubbles with radii smaller than 600 µm certainly such a location could be found.

The present study shows, however, that with a resolution of 11 µm for four model-scale conditions, a bubble radius smaller than 200 µm exists for which no such location can be found. This does not falsify the theoretical considerations in (Beelen and van Rijsbergen, 2018), but even if such a particular location exists, the chance that a bubble would cross exactly this position in an experiment is nearly zero. Therefore, it is proposed to return to the classical definition of bubble screening as an exclusion of bubbles above a certain initial radius that can cause cavitation inception. The process which – with increasing bubble radius – decreases the range of initial vertical positions from which bubbles can start induce sheet cavitation is designated as ‘bubble selection’. This process eventually leads to bubble screening.

The trends in the scale effects on bubble screening, found on the propeller blade section (see Figure 10) correspond qualitatively with those found by Johnson and Hsieh (1966). They found that the smaller the width of the body, the smaller the maximum radius of the bubble that hits the surface of the body upstream of the point of minimum pressure. Furthermore, the lower the free-stream velocity, the larger this maximum bubble radius becomes.

5.3 Scale effect on the minimum pressure

Figures 5 and 8 show that keeping the cavitation number constant in model-scale cavitation experiments results in a pressure equal to the vapour pressure at geometrically scaled locations, but also in a minimum pressure that is strongly dependent on the free-stream velocity. For most of the conditions studied here, this does not lead to scale effects in the bubble behaviour; the maximum attained bubble radii and distances between growth and collapse of the bubbles scale geometrically. On the smallest model-scale propeller, however, the bubble behaviour is clearly different from that on full scale (cf. Figures 7 and 9), due to a smaller pressure peak. It results in a maximum equivalent bubble radius of approximately 0.1 mm, which is significantly smaller than the (scaled) maximum radii on larger propellers.

A viscous scale effect on the minimum pressure – especially for this blade section with a sharp pressure peak – is expected to enhance the above-described phenomena: an even smaller pressure peak (in height and chord-wise extent), resulting in less bubble growth.

5.4 Scale effects on sheet cavitation inception

Van Rijsbergen and van Terwisga (2010) studied the sensitivity of cavitation inception to a variation of the rotation rate of propeller S (Kuiper, 1981) by experiments in MARIN's Depressurized Towing Tank, nowadays called Depressurized Wave Basin (DWB). They found a strong decrease in the radial cavitation extent (measure of the amount of cavitation) when the rotation rate was decreased from 10 to 7 Hz. In this condition, no nuclei were seeded, so only the natural nuclei content was present in the water. In the analysis of the observations, a conceptual model was used in which it was assumed that the maximum available bubble radius was 25 μm. This value was assumed to decrease to approximately 15 μm by bubble screening at n = 10 Hz. It was assumed that R_S decreased further with decreasing rotation rate. Together with an increase of the minimum initial bubble radius according to the Blake threshold, this would give a significant reduction in the available number of free-stream nuclei for sheet cavitation inception at 7 Hz. It was thought that this could explain the smaller radial cavitation extent. The present results of the Lagrangian tracking computations for the same propeller at the same conditions, however, show that bubble screening does not occur for $R_0 \leq 430$ μm (see Figures 3 and 4). This is significantly higher than the formerly estimated value of 15 μm. Also, the present study clearly shows that R_S increases with decreasing rotation rate.

Furthermore, van Rijsbergen and van Terwisga (2010) assumed an effective minimum pressure coefficient (C_{Pmin}) on the blade section of -1.9 on the basis of cavitation inception experiments and a correction for the effect of roughness. The Blake threshold was used to calculate the corresponding critical radius of a bubble. The initial bubble radius was assumed to be equal to the critical radius, which resulted in an overestimate of the initial radius with approximately a factor 2. The potential flow computation as used in the present study gives $C_{Pmin} = -5.4$, which gives much smaller minimum initial bubble radii that can cause sheet cavitation inception. However, viscous effects could increase the minimum pressure again. Therefore, it is recommended to use viscous flow computations in combination with the present Lagrangian tracking model to study the experimental findings further. Additionally, it is recommended to conduct nuclei measurements in open water condition in the DWB with the technique recently developed by Birvalski and Rijsbergen (2018). In particular, the bubble size vs. concentration spectra for different ambient pressures with and without seeding are required for a better understanding of the experimental conditions.

5.5 Sheet cavitation inception mechanisms

The range of initial bubble radii that could cause sheet cavitation on the smallest propeller model (5-160 μm), corresponds quite well with measured bubble distributions generated by electrolysis in the DWB (Birvalski and Rijsbergen, 2018). Therefore, only the range of bubble radii that can cause sheet cavitation inception on a propeller blade as obtained in the present study cannot explain scale effects on sheet cavitation inception. It is recommended to study this further using cavitation inception event rates based on the range of initial radii as well as the range of initial vertical positions and measured nuclei spectra. Finally, in the present study it is assumed that sheet cavitation is induced if any bubble (partly) hits the surface where the pressure is below the vapour pressure. This is a practical implementation of the state of knowledge on sheet cavitation inception, but many aspects of the inception process are still unknown (van Rijsbergen, 2016). Once the physical process is understood better, scale effects on sheet cavitation inception can be studied in a better way.

6 CONCLUDING REMARKS

- Bubble screening limits the maximum radius of a bubble that can cause sheet cavitation inception on the considered blade section on model scale to approximately 200 μm.
- The found decrease of the range of bubble radii that can induce cavitation inception with decreasing propeller diameter cannot explain scale effects on sheet cavitation inception.
- The (non-viscous) scale effect on the minimum pressure caused aberrant bubble behaviour for the smallest propeller diameter at the lowest rotation rate. It is not clear, however, if this affects the sheet cavitation inception process.
- The Lagrangian tracking method used in this study is a valuable tool to investigate cavitation inception mechanisms. Viscous flow computations which show the scale effects on the pressure distribution – and especially the minimum pressure – can further improve the present method.

REFERENCES

Beelen, S. and van Rijsbergen, M. X. (2018) 'Bubble screening in lifting flows and its effect on cavitation inception', in *Numerical Towing Tank Symposium (NuTTS)*. Cortona, Italy.

Billet, M. L. and Holl, J. W. (1981) 'Scale Effects on Various Types of Limited Cavitation', *Journal of Fluids Engineering*, 103(September), pp. 405–414.

Birvalski, M. and Rijsbergen, M. X. Van (2018) 'Application of Interferometric Particle Imaging to cavitation nuclei measurements in a ship model basin', in *19th International Symposium on the Application of Laser and Imaging Techniques to Fluid Mechanics*. Lisbon, Portugal.

Blake, J. R., Leppinen, D. M. and Wang, Q. (2015) 'Cavitation and bubble dynamics: the Kelvin impulse and its applications', *Interface Focus*. Royal Society, 5(5), p. 20150017.

Brennen, C. E. (1995) *Cavitation and bubble dynamics*. Oxford University Press.

Ceccio, S. L. and Brennen, C. E. (1991) 'Observations of the dynamics and acoustics of travelling bubble cavitation', *Journal of Fluid Mechanics*. 2006/04/26. Cambridge University Press, 233, pp. 633–660.

Gindroz, B. and Billet, M. L. (1998) 'Influence of the nuclei on the cavitation inception for different types of cavitation on ship propellers', *Journal of Fluids Engineering*. ASME, 120(1), pp. 171–178.

Guennoun, F. *et al.* (2003) 'Experimental investigation of a particular travelling bubble cavitation', in *5th International Symposium on Cavitation*. Osaka, Japan.

Johnson, V. E. and Hsieh, T. (1966) 'The influence of the trajectories of gas nuclei on cavitation inception', in *6th Symposium on Naval Hydrodynamics*, pp. 163–179.

Kuiper, G. (1981) *Cavitation inception on ship propeller models*. PhD Thesis, Delft University of Technology.

van Rijsbergen, M. X. (2016) 'A review of sheet cavitation inception mechanisms', in *International Symposium on Transport Phenomena and Dynamics of Rotating Machinery*. Honolulu, Hawaii.

van Rijsbergen, M. X. and van Terwisga, T. J. C. (2010) 'Water quality effects on sheet cavitation inception on a ship propeller model', in *7th International Conference on Multiphase Flow*. Tampa, Florida USA.

van Rijsbergen, M. X. and van Terwisga, T. J. C. (2011) 'High-speed micro-scale observations of nuclei-induced sheet cavitation', in *3rd International Cavitation Forum*. Warwick, UK.